A Versatile Emulator for Haptic Communication to Alter Human Gait Parameters

Mengnan Wu[1, *], Yingxin Qiu[2], Jun Ueda[2], Lena H. Ting[1,3]
[1]W. H. Coulter Department of Biomedical Engineering, Emory University and Georgia Institute of Technology, 30332-4250, Atlanta, USA
[2]George W. Woodruff School of Mechanical Engineering, Georgia Institute of Technology, 771 Ferst Drive, 30332-0405, Atlanta, USA
[3]Department of Rehabilitation Medicine, Division of Physical Therapy, Emory University, 30332-0425, Atlanta, USA
*corresponding author: mengnan.wu@emory.edu

***Abstract*— Robotic devices that interact with humans at the hands through haptic communication – instead of mechanical power transmission – represent an intuitive way to assist persons with physical disabilities and teach movement skills. Principles of human-human haptic communication during walking could inspire novel robot controllers capable of altering specific spatiotemporal gait parameters, not just walking speed. However, we know little about how hand interactions affect gait parameters, as existing hand-contact robots have several performance limitations that hinder rapid testing of different controllers and parameters. Here we present the design and validation of Slidey, a novel robotic testbed capable of emulating diverse hand interactions to alter human gait parameters. A lightweight, instrumented linear stage translating on a >5 m long track, Slidey allows overground walking at speeds ≤2.4 m/s; high-fidelity current and position control at >500 Hz and ~6 Hz, respectively; and stable rendering of a range of admittances (mass ≤10 kg, damping ≤20 N/(m/s)). We show proof-of-concept that Slidey has adequate functionality to target changes in step length or step frequency. Slidey can thus be a high-fidelity robotic emulator to rapidly investigate, evaluate, and personalize robot controllers to alter gait through haptic communication at the hand.**

Keywords—physical human-robot interaction, haptic communication, robotic emulator, hand interactions during walking

I. Introduction

Haptic communication – the use of touch for information transfer as opposed to mechanical power transmission [1] - at the hand represents a novel and intuitive approach to aid and alter human walking. This approach avoids exerting large loads on the person's body and does not require donning/doffing (as for example in wearable "exoskeletons"). The potential for subtle hand interactions to alter walking without explicit instructions are demonstrated in activities such as two people holding hands while walking or partner dancing. Studies on haptic communication have demonstrated that human pairs use low-force (2 N [2] to 30 N [3]) hand interactions during walking to synchronize gait phase [2], [4], signal walking transitions [3], and aid balance during walking [5].

Physical human-robot interactions (pHRI) have the potential to apply haptic communication principles used by humans to several walking applications, such as assistive technology for persons with visual or walking impairments and teaching movement skills (e.g. dance or sports activities) to persons with or without physical disabilities. However, in order to investigate and apply haptic communication principles, pHRI devices must be capable of emulating a wide range of human hand behaviors during walking.

A variety of custom, one-off hand-contact pHRI devices have been developed to be used during walking. These consist mostly of robotic walkers and canes (reviews in [6]–[9]), humanoid "dance" partners (e.g. [10]–[13]), and mobile haptic manipulation interfaces (e.g. [14], [15]). Very few of these devices have demonstrated effects on spatiotemporal gait parameters [16] crucial for understanding gait disorder mechanisms and appropriate interventions. Improvements in spatiotemporal gait parameters (compared to walking without the device) reported in hand-contact pHRI devices include increased gait speed [12], [17]–[20], increased step/stride length [17]–[19], and decreased step width [21]. However, the devices that have shown these effects on gait parameters combine a unique hardware design with a specific type of controller, making it difficult to distinguish the contributions of the hardware vs the controller to effects on human gait.

Specialized, mobile hand-contact pHRI devices typically have performance limitations that make them ill-suited for testing how different types of controllers influence human behavior. The device in [21] is not capable of online force control. The device in [20], [22] has a maximum speed of 1.2 m/s, and users expressed concern about device weight. The device in [19] has a maximum speed of 1.5 m/s and poor force sensing resolution. The humanoid robot in [12] weighs ~160 kg, has a maximum speed of 0.7 m/s, and shows severe bandwidth limitations (<2 Hz). System bandwidth may be especially important for rendering quick, small movements in haptic communication; hand torques for haptic communication during a non-walking task reach about 12 Hz [23]. However, controller performance was not validated for any of the devices in [17]–[22]. Heavy weight, low speed, and low bandwidth may be unavoidable for mobile robots that must transport motors and power supplies. While one fixed-in-space hand-contact pHRI device exists [18], [17], it requires use of a self-paced treadmill with its own controller, which may have unintended effects on spatiotemporal gait parameters.

Furthermore, existing devices have focused primarily on improving how fast people walk [17]–[19] but not how they coordinate gait parameters such as step frequency and step length as they change speeds. Altering gait parameters in a targeted manner is an important function for robots designed to assist persons with physical disabilities or teach movement skills. During unaided human gait there is a constant relationship between step frequency and step length [24], [25], but altering this "walk ratio" is necessary for different contexts such as walking on stepping stones or avoiding obstacles. Step

frequency and length relationships across gait speed are affected in a variety of motor pathologies, e.g. individuals with Parkinson's disease show difficulty modulating step length but not step frequency [26]. While some hand-contact pHRI devices have increased gait speed, this change was coupled to increased step/stride length [17]–[19] and did not change the relationship between step frequency and length.

In prosthetics and exoskeleton pHRI research, laboratory testbeds or "emulators" have been highly effective for quickly exploring a variety of device controllers and functionalities with fewer performance fidelity limitations compared to mobile, standalone devices [27]–[29]. Emulators enable direct testing of human responses to complex physical interactions in a manner not possible in purely computational simulations. Additionally, emulators have enabled human-in-the-loop optimization where the interaction between device parameters and the human's response are used to personalize assistance for different individuals [30], [31].

Thus, our goal was to build a versatile high-fidelity emulator capable of testing a wide range of controllers that use hand interactions to alter human gait parameters, especially controllers inspired by human-human haptic communication. Here we describe performance criteria and mechanical design of the emulator, "Slidey", a robotic handle that slides on a >5m linear track while the human user walks overground. We demonstrate that Slidey has adequate performance to emulate a range of hand interactions during walking under three different controllers: current control (equivalent to closed-loop control of motor force), position control, and admittance control. Finally, we demonstrate proof-of-concept that Slidey can decouple the coordination of the gait parameters step length and step frequency as gait speed increases in an unimpaired participant. We therefore show that Slidey has sufficient capabilities to be used as a robotic emulator to identify and test controllers that can be implemented in mobile robotic devices.

II. Device Design and Validation

A. Design criteria

A versatile emulator for physical human-robot hand interactions to alter gait parameters must allow for a wide range of human walking behavior while maintaining human safety. The use of a treadmill often enforces a constant walking speed, which is not typical of many activities of daily living [32]. Alternatively, to allow variable walking speed, an additional controller for the treadmill is necessary and potentially conflates with effects of the hand interaction controller. The robot must also be able to match maximum human gait speeds, which range up to 2.5 m/s [33]. Such a speed may be dangerous to achieve with a large robot, so an ideal emulator should be as lightweight as possible so that it has minimal momentum.

To emulate haptic communication, the device must also allow for a range of hand interactions during walking. To emulate existing hand-contact pHRI devices for altering walking, the device must be capable of force and admittance control. To emulate haptic communication during walking, the emulator must be capable of sensing small forces that range from 2 N [2] to 30 N [3]. Thus the hardware requires a precise force sensor with low noise to maintain stability, especially during admittance control. Furthermore, admittance control of the device should not result in forces >30 N in order to emulate human-human haptic communication.

Investigating haptic communication principles and testing biologically-inspired human-robot controllers requires sufficient bandwidth to match frequencies found in human movement. Normal human walking has a kinematic bandwidth of 4-6 Hz [34], and torques exerted at the hand for haptic communication during seated human-human upper-limb interactions reach about 12 Hz [23]. Thus the robot's bandwidth should be at least 6 Hz for position control and at least 12 Hz for force or torque control. Additionally, as human cutaneous mechanoreceptors can sense frequencies up to 1 kHz [35], robotic devices and controllers for pHRI should avoid unintentional vibrations in this range.

A prior study showed that humans prefer fewer degrees of freedom (i.e. very stiff arms and a compliant admittance-controlled base) [12] in a mobile humanoid robot partner, suggesting that a simple one-degree-of-freedom device is sufficient to examine principles of hand interactions in human-robot partnered walking.

B. Hardware design and specifications

In order to allow for overground walking across the range of possible human walking speeds while minimizing risk of injury to the human user, we chose a novel design that translates a sliding stage on a long fixed track for our emulator Slidey (Fig. 1). The maximum translational displacement of >5 m allows most humans to walk several steps. As opposed to a mobile robot, a device that moves on a fixed track also consumes less of the device's power for self-locomotion and can achieve high speeds (Slidey can achieve a translational speed of 2.4 m/s) while achieving high bandwidth control for emulating physical interactions with the human.

The linear stage slides on a one-degree-of-freedom track powered by a linear induction motor (Fig. 1). The linear stage has a 5.34 m stroke (model: 2XBLDM-B04, H2W

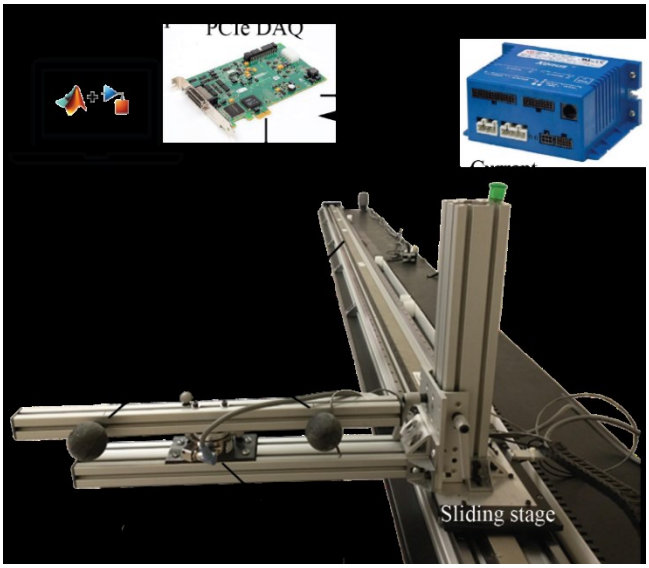

Fig. 1: Robotic emulator components and communication pathways

Technologies, Inc., CA, USA) controlled by a servo drive (Xenus XSJ-230-10, Copley Controls, MA, USA). The position of the linear stage is measured by a 1-um resolution linear encoder (LM10, Renishaw, Wotton-under-Edge, England). The motor has a 6.6 N/Amp motor constant and 166.6 N force output at 10% duty cycle. The servo drive is configured in current control mode that supports 4.43 Amp continuous current and 10 Amp peak current, resulting in approximately 55.2 N continuous force and 110 N peak force, well beyond that needed for haptic communication.

The user interface is designed to be ergonomic and versatile, allowing adjustability for different modes of use and users with varying anthropometric measurements. Two handles are attached to an aluminum bar (80/20, Columbia City, IN, USA) fixed to the sensing face of a 6-axis force-torque sensor (model: 9105-T-GAMMA SI-32.2.5, ATI Industrial Automation, NC, USA). The sensor is mounted on another aluminum bar fixed to the linear stage with an adjustable brake. Handles can be mounted on either side of the device, allowing forward walking in either direction, and one handle can be completed removed to test one-handed vs. bimanual hand interactions. The handles were custom-designed and 3D-printed to the shape and size of a doorknob. The location of each handle can be adjusted to accommodate different distances between the user's arms, up to 60 cm. The height of the handles can be adjusted 97-126 cm above ground level to allow each user to maintain a comfortable arm posture of elbows bent at 90 degrees and wrists flat.

The force-torque sensor meets specifications required for measuring and controlling forces in haptic communication. In the direction of walking, the force-torque sensor has a resolution of 6.25 mN, which is more than sufficient to measure the smallest human hand forces during walking. Electrical noise is <0.03 N pk-pk, which can be rejected by a force deadzone in the robot controller to maintain stability without losing relevant human-robot interaction data.

Multiple safety features are implemented via hardware design, analog circuitry, and digital controls. The design of a small moving stage on a fixed track is inherently safer than a large mobile robot, with the weight of all moving parts on Slidey totaling ~8.4 kg. While the device is not designed to support a person's bodyweight, if a large vertical force is exerted on the handles or aluminum bars, the most likely failure mode is that the brake for height adjustment would fall a maximum of 29 cm to the surface of the linear stage. The stage is mounted to a dual-track rail that can withstand 400 Nm in static moment loading, equivalent to ~110 kg - which exceeds average human bodyweight - loaded at the location of the force sensor. Custom safety features include a "dead-man's" switch embedded in one handle, which is depressed by the user's palm when holding the handle during normal operation. Letting go of the handle instantaneously shuts off power to the servo drive. Emergency stop buttons connected directly to the servo drive power are positioned at the main control computer and at the far end of the track. A 10 Amp fuse is installed in series with the servo drive power. An instantaneous velocity limit of 9 m/s is implemented in the servo drive software.

C. Control architecture

A high-speed, high-precision, hierarchical control scheme enables versatile robot control (Fig. 1). A dedicated Windows PC runs Simulink Desktop Real-Time (SDRT) software (Mathworks, MA, USA) and commands the servo drive, which runs a separate lower-level current controller. SDRT runs at 1kHz and outputs an analog voltage command via a 16-bit PCI DAQ board (PCIe6323, National Instruments, TX, USA) to the servo drive running at 15kHz, which converts the voltage signal to a current command at a 1:1 ratio with 12-bit resolution. We chose to use current control instead of position control in the low-level controller as to avoid loss of position resolution over the long stroke of the linear motor. Given a track length of 5.34 m, 12-bit resolution of the servo drive would result in a position command resolution of 1.2 mm, which we deemed insufficient for emulating smooth hand motions during walking. The servo drive acquires linear encoder data at 20 MHz. The force/torque sensor streams digital data at 7 kHz UDP over Ethernet (ATI Net F/T) to SDRT. Interaction force and encoder position are recorded at 1 kHz in SDRT.

For current control, SDRT sends desired current commands to the feedback controller for current (Fig. 2a) running on the servo drive. Custom Simulink code was written to realize position and admittance control. Closed-loop position control actual position from the digital encoder signal, and outputting a desired current command to the current controller (Fig. 2b). Admittance control is implemented by calculating desired position using the force sensor signal and chosen admittance is implemented by calculating desired position, comparing to values, and then outputting a desired position command to the position controller (Fig. 2c). For admittance control, we

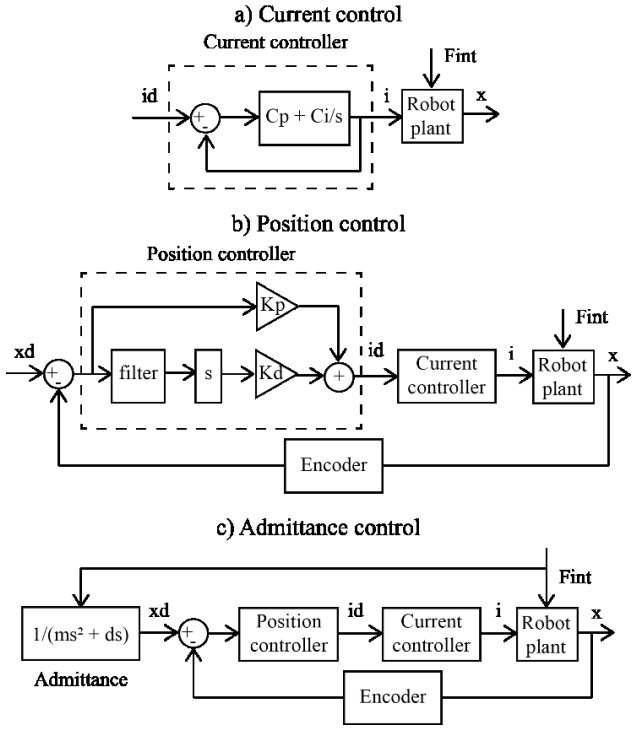

Fig. 2: Control diagrams for a) current control: *id* = desired current, *i* = actual current, *Cp* = proportional gain, *Ci* = integral gain, *Fint* = interaction force, *x* = actual position, b) position control: *xd* = desired position, *Kp* = proportional gain, *Kd* = derivative gain, and c) admittance control: *m* = virtual mass and *d* = virtual damping.

implemented a deadzone of +/- 0.5 N on the force signal to prevent effects of electrical noise, which could potentially destabilize the controller and threaten the user's safety.

D. Controller performance validation

1) Current control

The parameters for the current controller (Fig. 2a) on the servo drive were tuned using the auto-tuning function in CME2 software (Copley Controls, MA, USA), and we chose the software option to "maximize smoothness" of operation. The final tuning gains obtained were Cp = 61 and Ci = 40. To characterize the frequency response with these gains, we input sinusoids with amplitude of 2 Amps and frequencies logarithmically scaled between 1-1024 Hz and calculated bandwidth from the resulting Bode plot (Fig. 3). The -3dB bandwidth achieved was between 512 and 1024 Hz (or ~651 Hz from linear interpolation).

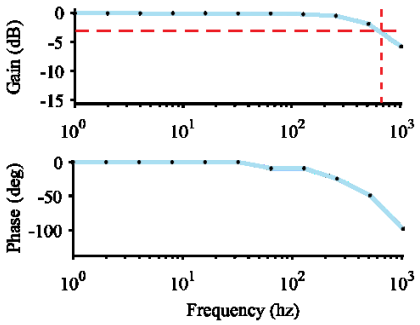

Fig. 3: Current controller Bode plot characterizing gain and phase between actual current output and desired current input. Dashed red line indicates the -3dB bandwidth. Data points plotted as black dots and connected with blue lines for visualization.

2) Position control

Feedback gains for the closed-loop position controller (Fig. 2b) were manually tuned to result in smooth motion without high-frequency vibrations when commanding both a constant velocity and velocity pulses. The tuning gains used were Kp = 80 and Kd = 30. The discrete filter on encoder position data had a transfer function of $100s/(s+100)$. As position commands from the high-level controller are converted into current commands at the low-level controller as described previously, we next calculated the bandwidth of our system based on desired position inputs and actual position outputs. We input sinusoids with a velocity amplitude of 0.2 m/s (which we found anecdotally to be sufficient for the human-subject experiment in Section III) and frequencies up to 20Hz and calculated the 3dB bandwidth from the resulting Bode plot (Fig. 4). The bandwidth achieved was 5.84 Hz. The system also does not have significant power in frequencies >10 Hz, which is important for avoiding high-frequency vibrations that can be sensed by human cutaneous mechanoreceptors.

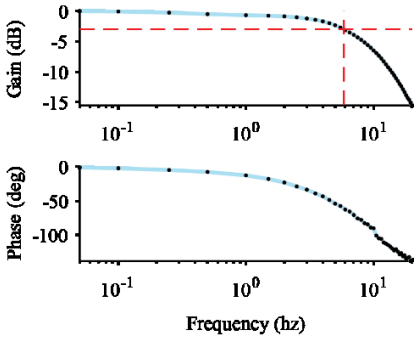

Fig. 4: Position controller Bode plot characterizing gain and phase between actual position output and desired position input. Dashed red line indicates the -3dB bandwidth. Data points plotted as black dots and connected with blue lines for visualization.

3) Admittance control

We validated our admittance controller by measuring actual (x) and desired (xd) position while a person held on to the handles of the device and exerted sinusoidal forces over a range of fixed frequencies during standing. While our device is capable of rendering a wider range of admittances (virtual mass ≤ 10 kg, virtual damping ≤ 20 N/(m/s)), we chose admittance values of 5 kg and 2.5 N/(m/s) for our validation based on responses from the human participant about when they felt the device followed them well during walking. Our validation data showed a correlation of r = 0.997 between actual and desired position with lag = 0.024s (Fig. 5a). Interaction forces remained within ranges realistic for haptic communication, i.e. < 30N in tension or compression (Fig. 5a). As the human could only move their arms/hands at a maximum frequency ~2 Hz, our Bode plot includes frequencies up to this limit.

Results show that we have adequate bandwidth for admittance control in a realistic range of human hand/arm motions, i.e. we achieved a gain of -0.69 dB or power ratio of 0.92 at 2 Hz (Fig. 5b). Our emulator's capability for rendering a wide range of admittance values with high fidelity will enable us to directly compare controller parameters in one hardware platform and personalize parameter values to individuals to maintain haptic communication force levels in future studies.

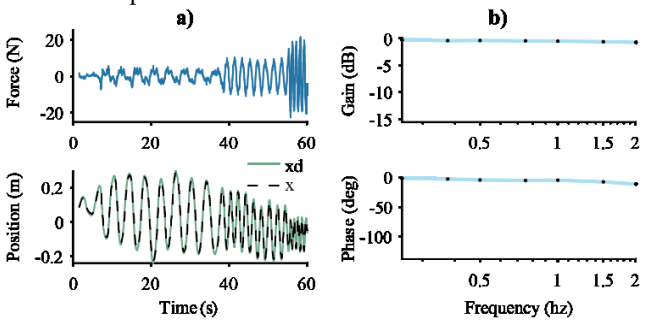

Fig. 5: Admittance control validation. a) Time series plots of sinusoidal force input (tension < 0) to robot from human upper limbs and desired (xd) and actual (x) robot position calculated for admittance values of mass = 5 kg and damping = 2.5 N/(m/s). b) Bode plot characterizing gain and phase between actual and desired position during sinusoidal force inputs. Data points plotted as black dots and connected with blue lines for visualization.

III. Proof-of-Concept Alteration of Spatiotemporal Gait Parameters Through Small Forces at the Hand

A. Velocity profile controller

As both force and admittance control have been demonstrated to alter human walking speed [12], [17]–[19], we focus on showing feasibility for using a novel velocity controller to alter coordination of gait parameters in addition to walking speed. Humans alter both step frequency and step length at a fixed ratio over a range of speeds during unaided walking [24], [25]. Here we sought to demonstrate that Slidey

has sufficient performance to enable future studies to systematically alter this ratio. Specifically, we tested whether interactions at the hand could preferentially increase step frequency or step length as walking speed increases.

We developed custom robot velocity profiles consisting of transient velocity pulses at varying frequencies superimposed on a constant velocity ramp of varying magnitude (which we term "bias") implemented via position control (Fig. 6a). We hypothesized that the robot's velocity bias (b) at the hand would affect average human walking speed (v) while the robot velocity pulse frequency (fR) would affect average human step frequency (f) (Fig. 6a, b). Given the relationship that average walking speed is the product of step frequency and step length (L), i.e. $v = f * L$, we varied the robot bias and pulse frequency to target changes in either human step frequency or step length.

Before the main experiment, we measured the participant's preferred gait speed, step frequency, and step length during overground walking without the robot. To control for effects of arm swing, we asked the participant to walk at preferred speed while maintaining an arm posture similar to that used with the robot (elbows bent at 90 degrees). We calculated gait speed using the first and second heelstrike events from motion capture data per trial. We then calculated mean values across 3 trials and used these values to normalize subsequent data.

The main experiment had 3 conditions (Alter Gait Speed, Alter Step Frequency, and Alter Step Length), at each of 3 desired gait speeds (Below, Equal to, and Above the individual's preferred speed from walking without the robot). Blocks of 5 trials were performed for each level of each condition, with order of blocks randomized.

TABLE I. EXPERIMENT CONDITIONS, LEVELS, AND DESIRED EFFECTS

Condition	Level		
	Below	Preferred	Above
Alter Gait Speed (v)	v ↓	v ←→	v ↑
	f ↓	f ←→	f ↑
	L ↓	L ←→	L ↑
Alter Step Frequency (f)	v ↓	v ←→	v ↑
	f ↓	f ←→	f ↑
	L ←→	L ←→	L ←→
Alter Step Length (L)	v ↓	v ←→	v ↑
	f ←→	f ←→	f ←→
	L ↓	L ←→	L ↑

In the Alter Gait Speed condition, only velocity bias without pulses was change to enforce gait speed changes. This condition established the baseline ratio between step frequency and step length for comparison to the pulsed conditions.

The pulsed conditions aimed to alter either step frequency or step length with walking speed. During Alter Step Frequency conditions, robot velocity pulse frequency was set to desired human step frequency ($fR = f$). To maintain a constant step length, we scaled robot velocity (vR) based on the relationship between walking speed, step frequency, and step length (i.e. set $vR = v = f * L = fR * L$). During the Alter Step Length condition, we set the ratio between velocity bias and pulse frequency (b/fR) to achieve a desired step length, while maintaining a constant step frequency by fixing fR. Desired changes in human gait parameters are summarized in Table 1.

B. Experiment setup

A young adult (age 27 years, height 1.85 m, weight 106 kg) without neurological or physical impairments was recruited from Emory University (IRB00082414) to participate in user testing. Retroreflective markers were attached to the participant's body according to the Lower Body Plug-in-Gait model with an additional marker at the left shoulder and recorded at 120 Hz with a 10-camera motion capture system (Vicon Nexus, Oxford, UK). Gait parameters of walking speed, step frequency, and step length were calculated from motion capture data of shoulder and heel markers (Fig. 6b, c).

Because we wish to develop a robot that is intuitive to use, the participant was not given explicit instructions on how to walk with the robot other than to maintain arm/hand posture (elbows bent at 90 degrees, holding the robot handles "like doorknobs") and step with the left foot first. At the start of each trial, the participant was instructed to maintain a consistent standing posture with weight mostly on the right foot, and to "get ready to walk" after a series of auditory beeps. To remove auditory and visual cues from the robot, the participant wore headphones playing white noise and was instructed to look straight ahead, not at the robot.

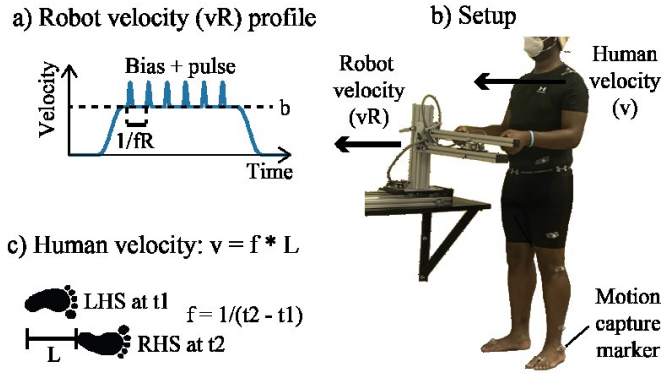

Fig. 6: Experiment design. a) Custom velocity profiles with velocity bias "b" and transient pulses at frequency "fR." were implemented in the robotic emulator to alter specific gait parameters. b) Participant kinematics were recorded via motion capture while they held the hand of the device and walked forwards. c) Human gait parameters of gait speed (v), step frequency (f), and step length (L) were calculated from motion capture data (LHS = left heelstrike, RHS = right heelstrike, t1 = time of LHS, t2 = time of RHS).

C. Data Analysis

We calculated gait parameters based on kinematics between the second and seventh heelstrike events of each trial to exclude gait initiation and termination. Foot velocity was visually inspected to ensure that steady-state walking speed was reached. All motion capture marker data was lowpass filtered at 30Hz. Gait speed was calculated from the left shoulder marker's displacement over the steady state walking period. Step frequency was calculated from time between consecutive heelstrike events, averaged across all heelstrikes during the steady state walking period per trial. Step length was calculated as distance between heel markers at each heelstrike, averaged across all heelstrikes during the steady state walking

period per trial. We normalized gait speed, step frequency, and step length by values obtained from overground walking without the robot.

To test if the participant altered the ratio between step frequency and step length, we compared regression slopes of step frequency vs. step length data for the three experiment conditions. We compared slopes from the pulsed conditions (Alter Step Frequency and Alter Step Length) vs. the slope from the unpulsed Alter Gait Speed condition to test if we manipulated walk ratios away from the preferred baseline value across a range of gait speeds. Significant differences between slopes for different conditions were tested by examining the 95% CI's of regression coefficients.

Finally, we examined relationships between hand interaction force and foot velocity to better understand *how* hand interactions affect walking kinematics. Force data was downsampled to match sampling frequency for motion capture data. We obtained the anterior-posterior velocity for each foot from differentiating heel marker positions and then added the left and right velocities for combined foot velocity. After detrending and lowpass filtering both force and foot velocity data at 30Hz, we performed cross-correlation on the two signals during the steady state walking period and obtained the time lag at maximum correlation.

D. Results

Kinematic results show that the pulsed robot velocity conditions resulted in intended changes in the ratio between step frequency and step length vs. the baseline unpulsed condition. Step frequency and step length increase at a fixed ratio as gait speed increases during the Alter Gait Speed control condition (blue data points and regression line in Fig. 7). Step frequency is preferentially altered with gait speed during the Alter Step Frequency condition (red in Fig. 7), as seen in the steeper regression line slope compared to the control condition. Step length is preferentially altered with gait speed during the Alter Step Length condition (yellow in Fig. 7), as seen in the shallower regression line slope compared to control. Due to the large variability in step frequency and length at slow gait speeds, we also performed regression without data from the Below level for each condition and found statistically significant differences in slopes between the Alter Step Length condition and the other two conditions (Fig. 7b).

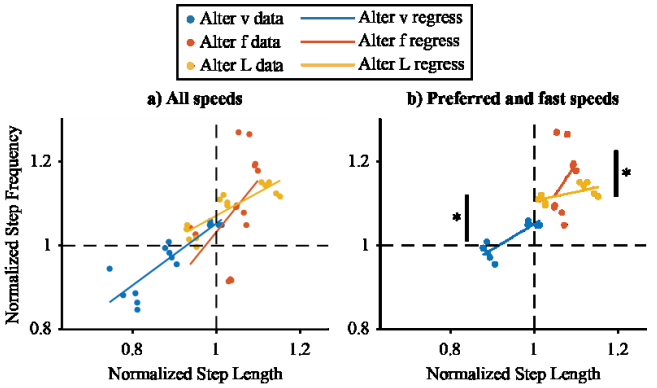

Fig. 7: Changes in ratio between step frequency and step length in robot velocity pulse conditions. Color denotes gait parameter targeted. Dots denote individual trial data; lines denote linear regression to trial data. (*) indicates significantly different regression line slopes. Step frequency and step length are normalized to the participant's preferred values when walking without the robot. a) Regression including all levels of each condition. b) Regression excluding levels below preferred values results in significant differences in slopes.

Unintentionally, gait speeds for the pulsed conditions were higher than the speeds for the control condition without pulses, so the ranges of step frequency and step length are also larger for the pulsed conditions. The velocity pulses may have contributed to average gait speed in addition to the bias magnitude, and the bias can be adjusted in the future to match gait speed ranges across all conditions.

Finally, we observed transient peaks in anterior-posterior (AP) hand force that were correlated in timing with AP foot velocity during the Alter Step Frequency condition (Fig. 8). Correlation between foot velocity and hand force was strongest when robot pulse frequency was at preferred step frequency (mean $r = 0.72$) and weaker when pulse frequency was below (mean $r = 0.52$) or above (mean $r = 0.59$) preferred step frequency. Foot velocity lagged hand force slightly (mean lag = 0.17 s) when hand pulse frequency was at preferred step frequency. Foot velocity tended to lag hand force more (mean lag = 0.22 s) when hand pulse frequency was above preferred step frequency. In contrast, foot velocity led hand force when hand pulse frequency was below preferred step frequency (mean lag = -0.55 s).

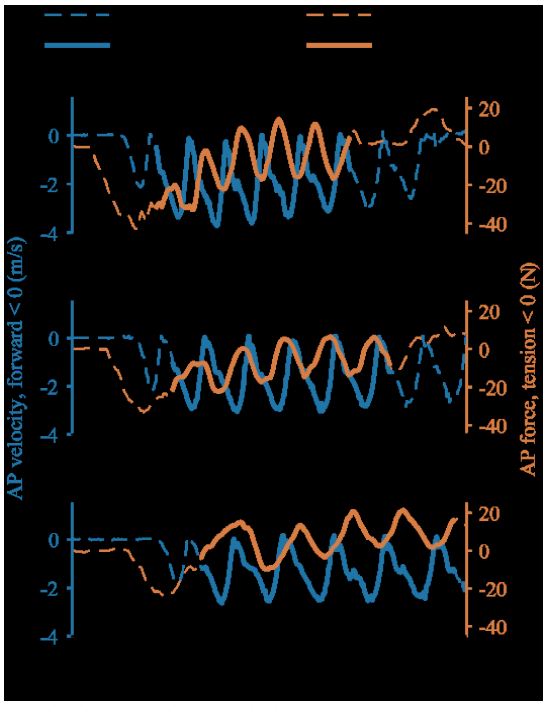

Fig. 8: Sample data for each level of Alter Step Frequency. Cross-correlation between condition combined (left + right) foot velocity and hand interaction force was calculated during steady-state for each trial.

IV. Discussion

To our knowledge, this is the first pHRI robot capable of being used as a platform for emulating a wide range of physical interactions at the hand during walking. The establishment of a versatile emulator for testing and studying physical interactions at the hand during overground walking can enable direct systematic comparison of the effects of different controller architectures. The high fidelity performance of the

robot is essential for rigorously identifying the effects of robot controllers on human gait behaviors, enabling new principles of human-robot interactions to be determined. Our emulator can further be used to develop and test novel physical interaction controllers based on human-human haptic communication. Finally, the ability to modify closed-loop human-robot interactions enable human-in-the-loop optimization of parameters for personalized assistance. Taken together, the novel functionalities offered by Slidey can enable rapid testing and prototyping of device functionalities to guide the design of mobile robots that use hand interactions to alter gait.

By allowing a variety of different controllers to be implemented with high fidelity, our versatile emulator enables future studies to design and compare controllers that may currently be limited to specific hardware platforms. The lightweight handle mounted on a long fixed track reduces the inertia of the system, enabling it to emulate motions (~6 Hz) and forces (>500 Hz) within the bandwidths observed in human walking and haptic communication, respectively, and can render a wide range of admittances (virtual mass ≤ 10 kg, virtual damping ≤ 20 N/(m/s)). Thus, we have the capability to both directly compare controllers from existing one-off devices in one hardware platform and perform experiments to test principles of human-robot haptic communication. This versatile emulator will help identify critical aspects of mobile robot performance necessary to achieve desired effects with the user.

As an example application, we show the feasibility of using the emulator not just to change how fast a person walks, but also how they coordinate their stepping patterns. The purpose of the single-user study was to show that the robot has the appropriate functionality to facilitate future experiments testing physical human-robot interactions for altering specific gait parameters. By changing the spatiotemporal patterns of robot motion, we demonstrate the capability to preferentially alter step frequency or step length with gait speed. Furthermore, the effects were achieved without explicit instructions to the user, showing the potential for intuitive robotic devices that require little to no training on the part of the user. The initial, proof-of-concept velocity trajectory controller used is not intended to be implemented on a mobile robot, but it demonstrates a starting point for development of more sophisticated control architectures and personalized control parameters necessary for robust human-robot haptic communication during gait. The versatility of our emulator will make such controller optimization and personalization simpler and faster to perform compared to existing specialized pHRI devices.

Our emulator also establishes a tool for scientific studies investigating causal relationships between hand interaction forces and gait parameters that could be leveraged in future robot control designs. Instrumented passive walkers show that hand/arm forces are related to spatiotemporal gait parameters [36], [37], and human-human partnered stepping show that forces at the hand can be used to guide the direction, timing, and magnitude of steps. However, identifying the causal nature of these effects requires the ability to systematically control and perturb the interaction using a well-controlled robotic device to test candidate hypotheses. For instance, our preliminary data show that forces at the hand are nearly time-synchronized with foot motions when the robot velocity pulses at the preferred step frequency and either lag or lead foot motions when robot pulse frequency is below or above preferred step frequency, respectively. More rigorous experiments can be conducted using Slidey to determine whether hand forces are due to the user anticipating versus reacting to the hand interactions.

In conclusion, our new robotic emulator Slidey can be used to implement, discover, and test a variety of controllers for pHRI to alter walking. Specifically, it can be used to emulate strategies of haptic communication not previously explored in pHRI and to develop and optimize novel controllers to target specific changes in spatiotemporal gait parameters. Developing a high-fidelity robotic emulator is a critical step towards better understanding of pHRI principles and for improving controller design for mobile pHRI devices that have the potential to assist persons with physical disabilities and teach movement skills to persons with or without disabilities.

ACKNOWLEDGMENT

The authors thank the Neuromechanics Lab. This work was funded by the National Science Foundation Division of Civil, Mechanical, and Manufacturing Innovation Mind, Machine, and Motor Nexus (M3X): NSF CMMI 1762211 and 1761679.

REFERENCES

[1] R. P. R. D. van der Wel, G. Knoblich, and N. Sebanz, "Let the force be with us: Dyads exploit haptic coupling for coordination.," *Journal of Experimental Psychology: Human Perception and Performance*, vol. 37, no. 5, pp. 1420–1431, 2011, doi: 10.1037/a0022337.

[2] F. Sylos-Labini, A. d'Avella, F. Lacquaniti, and Y. Ivanenko, "Human-Human Interaction Forces and Interlimb Coordination During Side-by-Side Walking With Hand Contact," *Front. Physiol.*, vol. 9, p. 179, Mar. 2018, doi: 10.3389/fphys.2018.00179.

[3] A. Sawers, T. Bhattacharjee, J. L. McKay, M. E. Hackney, C. C. Kemp, and L. H. Ting, "Small forces that differ with prior motor experience can communicate movement goals during human-human physical interaction," *J NeuroEngineering Rehabil*, vol. 14, no. 1, p. 8, Jan. 2017, doi: 10.1186/s12984-017-0217-2.

[4] A. Z. Zivotofsky and J. M. Hausdorff, "The sensory feedback mechanisms enabling couples to walk synchronously: An initial investigation," *Journal of NeuroEngineering and Rehabilitation*, vol. 4, no. 1, p. 28, Aug. 2007, doi: 10.1186/1743-0003-4-28.

[5] M. Wu, L. Drnach, S. M. Bong, Y. S. Song, and L. H. Ting, "Human-Human Hand Interactions Aid Balance During Walking by Haptic Communication," *Frontiers in Robotics and AI*, vol. 8, p. 357, 2021, doi: 10.3389/frobt.2021.735575.

[6] M. M. Martins, C. P. Santos, A. Frizera-Neto, and R. Ceres, "Assistive mobility devices focusing on Smart Walkers: Classification and review," *Robotics and Autonomous Systems*, vol. 60, no. 4, pp. 548–562, Apr. 2012, doi: 10.1016/j.robot.2011.11.015.

[7] M. Martins, C. Santos, A. Frizera, and R. Ceres, "A review of the functionalities of smart walkers," *Medical Engineering & Physics*, vol. 37, no. 10, pp. 917–928, Oct. 2015, doi: 10.1016/j.medengphy.2015.07.006.

[8] C. Werner, P. Ullrich, M. Geravand, A. Peer, and K. Hauer, "Evaluation Studies of Robotic Rollators by the User Perspective: A Systematic Review," *Gerontology*, vol. 62, no. 6, pp. 644–653, 2016, doi: 10.1159/000444878.

[9] S. Page, L. Saint-Bauzel, P. Rumeau, and V. Pasqui, "Smart walkers: an application-oriented review," *Robotica*, vol. 35, no. 6, pp. 1243–1262, Jun. 2017, doi: 10.1017/S0263574716000023.

[10] D. F. Paez Granados and K. Kosuge, "Design of a Male-type Dance Partner Robot for leading a physical Human-Robot Interaction," in *2015 IEEE International Conference on Mechatronics and Automation (ICMA)*, Aug. 2015, pp. 1234–1240. doi: 10.1109/ICMA.2015.7237662.

[11] J. Hölldampf, A. Peer, and M. Buss, "Synthesis of an interactive haptic dancing partner," in *19th International Symposium in Robot and Human Interactive Communication*, Sep. 2010, pp. 527–532. doi: 10.1109/ROMAN.2010.5598616.

[12] T. L. Chen *et al.*, "Evaluation by Expert Dancers of a Robot That Performs Partnered Stepping via Haptic Interaction," *PLoS ONE*, vol. 10, no. 5, p. e0125179, 2015, doi: 10.1371/journal.pone.0125179.

[13] T. L. Chen *et al.*, "Older adults' acceptance of a robot for partner dance-based exercise," *PLoS ONE*, vol. 12, no. 10, p. e0182736, Oct. 2017, doi: 10.1371/journal.pone.0182736.

[14] A. Bussy, P. Gergondet, A. Kheddar, F. Keith, and A. Crosnier, "Proactive behavior of a humanoid robot in a haptic transportation task with a human partner," in *2012 IEEE RO-MAN: The 21st IEEE International Symposium on Robot and Human Interactive Communication*, Sep. 2012, pp. 962–967. doi: 10.1109/ROMAN.2012.6343874.

[15] A. Peer and M. Buss, "A New Admittance-Type Haptic Interface for Bimanual Manipulations," *IEEE/ASME Transactions on Mechatronics*, vol. 13, no. 4, pp. 416–428, Aug. 2008, doi: 10.1109/TMECH.2008.2001690.

[16] O. Beauchet *et al.*, "Guidelines for Assessment of Gait and Reference Values for Spatiotemporal Gait Parameters in Older Adults: The Biomathics and Canadian Gait Consortiums Initiative," *Frontiers in Human Neuroscience*, vol. 11, 2017, Accessed: May 02, 2022. [Online]. Available: https://www.frontiersin.org/article/10.3389/fnhum.2017.00353

[17] G. U. Sorrento, P. S. Archambault, and J. Fung, "Adaptation and post-adaptation effects of haptic forces on locomotion in healthy young adults," *Journal of NeuroEngineering and Rehabilitation*, vol. 15, no. 1, p. 20, Mar. 2018, doi: 10.1186/s12984-018-0364-0.

[18] G. U. Sorrento, P. S. Archambault, J. Fung, and C. Feil-Oberfeld, "The effects of haptic forces on locomotion and posture in post-stroke and elderly adults," in *2015 International Conference on Virtual Rehabilitation (ICVR)*, Jun. 2015, pp. 147–148. doi: 10.1109/ICVR.2015.7358622.

[19] H. Lee *et al.*, "Development of a Robotic Companion to Provide Haptic Force Interaction for Overground Gait Rehabilitation," *IEEE Access*, vol. 8, pp. 34888–34899, 2020, doi: 10.1109/ACCESS.2020.2973672.

[20] R. Annicchiarico, "Enhancing service delivering, improving quality of life, preserving independence through assistive technology.," in *MIE*, 2012, pp. 14–18.

[21] D. M. Stramel, R. M. Carrera, S. A. Rahok, J. Stein, and S. K. Agrawal, "Effects of a Person-Following Light-Touch Device During Overground Walking With Visual Perturbations in a Virtual Reality Environment," *IEEE Robotics and Automation Letters*, vol. 4, no. 4, pp. 4139–4146, Oct. 2019, doi: 10.1109/LRA.2019.2931267.

[22] V. Kulyukin, A. Kutiyanawala, E. LoPresti, J. Matthews, and R. Simpson, "iWalker: Toward a Rollator-Mounted Wayfinding System for the Elderly," in *2008 IEEE International Conference on RFID*, Apr. 2008, pp. 303–311. doi: 10.1109/RFID.2008.4519363.

[23] K. B. Reed, M. Peshkin, M. J. Hartmann, J. E. Colgate, and J. Patton, "Kinesthetic interaction," in *9th International Conference on Rehabilitation Robotics, 2005. ICORR 2005.*, Jun. 2005, pp. 569–574. doi: 10.1109/ICORR.2005.1502027.

[24] N. Sekiya, H. Nagasaki, H. Ito, and T. Furuna, "The invariant relationship between step length and step rate during free walking," *Journal of Human Movement Studies*, vol. 30, no. 6, pp. 241–257, 1996.

[25] B. Bogen, R. Moe-Nilssen, A. H. Ranhoff, and M. K. Aaslund, "The walk ratio: Investigation of invariance across walking conditions and gender in community-dwelling older people," *Gait & Posture*, vol. 61, pp. 479–482, Mar. 2018, doi: 10.1016/j.gaitpost.2018.02.019.

[26] M. E. Morris, R. Iansek, T. A. Matyas, and J. J. Summers, "Ability to modulate walking cadence remains intact in Parkinson's disease.," *Journal of Neurology, Neurosurgery & Psychiatry*, vol. 57, no. 12, pp. 1532–1534, Dec. 1994, doi: 10.1136/jnnp.57.12.1532.

[27] J. M. Caputo and S. H. Collins, "A Universal Ankle–Foot Prosthesis Emulator for Human Locomotion Experiments," *Journal of Biomechanical Engineering*, vol. 136, no. 3, Feb. 2014, doi: 10.1115/1.4026225.

[28] Y. Ding, I. Galiana, A. Asbeck, B. Quinlivan, S. M. M. De Rossi, and C. Walsh, "Multi-joint actuation platform for lower extremity soft exosuits," in *2014 IEEE International Conference on Robotics and Automation (ICRA)*, May 2014, pp. 1327–1334. doi: 10.1109/ICRA.2014.6907024.

[29] B. T. Quinlivan *et al.*, "Assistance magnitude versus metabolic cost reductions for a tethered multiarticular soft exosuit," *Science Robotics*, vol. 2, no. 2, p. eaah4416, Jan. 2017, doi: 10.1126/scirobotics.aah4416.

[30] J. Zhang *et al.*, "Human-in-the-loop optimization of exoskeleton assistance during walking," *Science*, vol. 356, no. 6344, pp. 1280–1284, Jun. 2017, doi: 10.1126/science.aal5054.

[31] R. W. Jackson and S. H. Collins, "An experimental comparison of the relative benefits of work and torque assistance in ankle exoskeletons," *Journal of Applied Physiology*, vol. 119, no. 5, pp. 541–557, Sep. 2015, doi: 10.1152/japplphysiol.01133.2014.

[32] B. C. Glaister, G. C. Bernatz, G. K. Klute, and M. S. Orendurff, "Video task analysis of turning during activities of daily living," *Gait & Posture*, vol. 25, no. 2, pp. 289–294, Feb. 2007, doi: 10.1016/j.gaitpost.2006.04.003.

[33] R. W. BOHANNON, "Comfortable and maximum walking speed of adults aged 20—79 years: reference values and determinants," *Age and Ageing*, vol. 26, no. 1, pp. 15–19, Jan. 1997, doi: 10.1093/ageing/26.1.15.

[34] R. Khusainov, D. Azzi, I. E. Achumba, and S. D. Bersch, "Real-Time Human Ambulation, Activity, and Physiological Monitoring: Taxonomy of Issues, Techniques, Applications, Challenges and Limitations," *Sensors (Basel, Switzerland)*, vol. 13, no. 10, p. 12852, Oct. 2013, doi: 10.3390/s131012852.

[35] S. Mack, E. R. Kandel, T. M. Jessell, J. H. Schwartz, S. A. Siegelbaum, and A. J. Hudspeth, *Principles of Neural Science, Fifth Edition*. McGraw Hill Professional, 2013.

[36] M. Alwan, A. Ledoux, G. Wasson, P. Sheth, and C. Huang, "Basic walker-assisted gait characteristics derived from forces and moments exerted on the walker's handles: Results on normal subjects," *Medical Engineering & Physics*, vol. 29, no. 3, pp. 380–389, Apr. 2007, doi: 10.1016/j.medengphy.2006.06.001.

[37] A. Abellanas, A. Frizera, R. Ceres, and J. A. Gallego, "Estimation of gait parameters by measuring upper limb–walker interaction forces," *Sensors and Actuators A: Physical*, vol. 162, no. 2, pp. 276–283, Aug. 2010, doi: 10.1016/j.sna.2010.05.020.